



HAL
open science

Using spectral analysis to detect singular events such as jerks in the geomagnetic field time series

B. Duka, A. de Santis, M. Manda, A. Isac, E. Qamili

► To cite this version:

B. Duka, A. de Santis, M. Manda, A. Isac, E. Qamili. Using spectral analysis to detect singular events such as jerks in the geomagnetic field time series. *Solid Earth Discussions*, 2011, 3, pp.615-654. 10.5194/sed-3-615-2011 . insu-03606459

HAL Id: insu-03606459

<https://insu.hal.science/insu-03606459>

Submitted on 12 Mar 2022

HAL is a multi-disciplinary open access archive for the deposit and dissemination of scientific research documents, whether they are published or not. The documents may come from teaching and research institutions in France or abroad, or from public or private research centers.

L'archive ouverte pluridisciplinaire **HAL**, est destinée au dépôt et à la diffusion de documents scientifiques de niveau recherche, publiés ou non, émanant des établissements d'enseignement et de recherche français ou étrangers, des laboratoires publics ou privés.



Distributed under a Creative Commons Attribution 4.0 International License

Abstract

In this study we have applied two spectral techniques in terms of Fourier and wavelet analysis to geomagnetic field time series and compared the results with those obtained from analogous analyses to synthetic data. Then, an algorithm has been proposed to detect the geomagnetic jerks in time series, mainly being considered by the Eastern component secular variation. Applying such analysis to time series generated from global models has allowed us to depict the most important space-time features of the geomagnetic jerks on global scale, since the beginning of XXth century. Finally, a spherical harmonic analysis of the secular acceleration power spectrum has been computed since 1960 to 2000, bringing new insights in understanding these rapid changes of the geomagnetic field and their origin.

1 Introduction

Studies of discrete time-series of different physical quantities are of a huge interest not only for their forecasting, but also for defining the nature and behavior of the underlying physical phenomena. Different methods of time-series analyses are used here to study the geomagnetic field which is, at all times, subject to temporal variations on a wide range of time scales. Most of the rapid variations originate in solar activity and solar variability (many different forms including solar flares, coronal mass ejections, solar wind sector boundaries, coronal hole streams), as well as in the Earth's environment (interactions between the solar wind and the core field). Most of the slowest variations are generated in the outer core (changes in the fluid flow), The temporal variations in the geomagnetic field cover a huge range of time-scales, from seconds to hours (external in origin), from months to decades (overlapping between external and internal changes), or from millennial to reversals (internal variations). Here, we focus on the analysis of changes in geomagnetic field, as mainly observed from magnetic observatories. This work is dedicated to analyze the short-term (likely internal) variations, observed in the geomagnetic field.

Using spectral analysis to detect singular events

B. Duka et al.

Title Page

Abstract

Introduction

Conclusions

References

Tables

Figures



Back

Close

Full Screen / Esc

Printer-friendly Version

Interactive Discussion



time series analyses, while the third one is a global spherical harmonic analysis. In this paper, we present the results of applying these methods on time-series of geomagnetic field of different observatories or time-series of synthetic data generated by different models. Thereafter, we discuss the main results, their implications in understanding the deep Earth's interior, and finally we conclude.

2 Data: observed and model-based temporal series

Before presenting the applied methods, we summarize the used data. The first kind of dataset is superior due to its length and quality: it is composed by time-series of geomagnetic field components recorded in the geomagnetic observatories on the Earth. They are chosen to be longer than 50 yr and placed as far as possible from each other. In addition, some synthetic data have been generated by means of specific functions to simulate geomagnetic jerks, in order to find the better way of the real data processing. We then generated time-series of geomagnetic field components, secular variation (SV) or secular acceleration (SA) from two geomagnetic field models described below, for a regular (uniform) grid of points over the Earth. The latter allowed us to see specific large scale behaviors of jerks over the globe. We also used the models to investigate the secular acceleration of their Gauss coefficients.

2.1 Observatory data

In this work, we have considered several observatories: Alibag (ABG), Apia (API), Chambon La Foret (CLF), Eskdalemuir (ESK), Gnangara (GNA), Hermanus (HER), Huancayo (HUA), Kakioka (KAK), Lerwick (LER), Pilar (PIL), Sitka (SIT), Vassouras (VSS), for which hourly means have been downloaded from the site SPIDR of National Geophysical Data Center (NGDC) in the format WDC. From the original hourly means of these observatories, their monthly mean values series have been also calculated.

SED

3, 615–654, 2011

Using spectral analysis to detect singular events

B. Duka et al.

Title Page

Abstract

Introduction

Conclusions

References

Tables

Figures

◀

▶

◀

▶

Back

Close

Full Screen / Esc

Printer-friendly Version

Interactive Discussion



2.1.1 A typical time-series – Niemegek observatory

A long and typical time-series the geomagnetic field has been recorded at Niemegek Observatory. The annual means series of X-, Y-, Z-components and the differences of sequential values ($\Delta X/\Delta t$, $\Delta Y/\Delta t$, $\Delta Z/\Delta t$, with $\Delta t = 1$ yr) are presented in Fig. 1. The monthly means series of X-, Y-, Z-components show the same behavior of annual means, but the differences of sequential values ($\Delta X/\Delta t$, $\Delta Y/\Delta t$, $\Delta Z/\Delta t$, with $\Delta t = 1$ month), show that they are bearing a great amount of noise not filtered from the signal. Therefore, to remove most of the uncorrelated noise, we then applied a moving average (Olsen and Manda, 2007) to calculate a smoothed SV (see discussion in Sect. 3.2.3). A glance at these plots underlines a few remarks. First, the same field component has the same behavior in both time-series. However, mainly for the X-component the noise level is higher in the monthly means. Second, the secular variation presents changes in its trend in the annual curves and less clear in the monthly ones.

2.1.2 Some key observatories

Amongst the considered observatories, 4 of them shown in the Table 1 have been chosen as representatives for our analyses. These observatories have been selected because they have longer and uninterrupted series of recordings, and are located at different latitudes and longitudes.

Although all the components of geomagnetic field have been studied, we will present below mainly the results for the Y-component.

2.2 Geomagnetic models

Time-series of the geomagnetic field components, their SV and SA are generated from two of most known models, i.e. CM4 (Sabaka et al., 2004) and Gufm1 models (Jackson et al., 2000). In the following, before to go into the details of the analyses, we will introduce and describe the two models.

Using spectral analysis to detect singular events

B. Duka et al.

Title Page

Abstract

Introduction

Conclusions

References

Tables

Figures



Back

Close

Full Screen / Esc

Printer-friendly Version

Interactive Discussion



2.2.1 CM4 model

The CM4 model (Sabaka et al., 2004) entails the parameterisation and coestimation of fields associated with the major magnetic field sources in the near-Earth regime from field measurements taken from ground-based observatories and satellite missions (POGO, Magsat, Ørsted, CHAMP). It supplies the local X-, Y-, Z-components of the B field vector from the main, lithosphere, primary and induced magnetosphere, primary and induced ionosphere, and toroidal field sources. Two evaluations of the main field are accommodated per two given spherical harmonic degree ranges for the span period 1960–2000. Using the provided FORTRAN codes of this model (http://core2.gsfc.nasa.gov/CM/CM4_A.html), we have calculated monthly time-series of Cartesian components and their SV of the main field for different places of a regular grid on the Earth's surface. These computer codes supply even time-series of the Gauss coefficients, and their first, second, third, and fourth derivatives. The capacity of this model to represent geomagnetic jerks has been already investigated (Sabaka et al., 2002; Chambodut and Manda, 2005).

2.2.2 Gufm1 model

The gufm1 model (Jackson et al., 2000), is based on a massive compilation of historical observations of the geomagnetic field (from 1590 to 1990). For the period before 1800, more than 83 000 individual observations of magnetic declination were recorded at more than 64 000 locations; more than 8000 new observations come from the 17th century alone. Since no intensity data are available prior to 1840, the axial dipole component is linearly extrapolated back before this date. The time-dependent field model constructed from this dataset is parameterised spatially in terms of spherical harmonics and temporally in B-splines, using a total of 36 512 parameters. Using fortran codes of this model (<http://jupiter.ethz.ch/~cfinlay/gufm1.html>), we have generated monthly values series of X-, Y-, Z-components and their secular variations at points of a regular grid on the Earth's surface.

Using spectral analysis to detect singular events

B. Duka et al.

Title Page

Abstract

Introduction

Conclusions

References

Tables

Figures



Back

Close

Full Screen / Esc

Printer-friendly Version

Interactive Discussion



3 Methods: characteristics and application to datasets

3.1 Short Time Fourier Transform (STFT)

3.1.1 STFT – definition and representation

It is well known, that the Fourier analysis breaks down a signal into constituent harmonics of different frequencies. For regularly sampled data, Fourier analysis is performed using the discrete Fourier transform (DFT). The fast Fourier transform (FFT) is an efficient algorithm for computing the DFT of an input sequence x of length N . The output of DFT is a vector X with length N (Oppenheim and Schaffer, 1989):

$$X(k) = \sum_{n=1}^N x(n)e^{-i2\pi(k-1)(n-1)/N}; \quad 1 \leq k \leq N \quad (1)$$

The magnitude of $|X|^2$ is called the spectrum power and its plot versus frequency is a “periodogram”. Hereafter to remind the length of a vector we will put its length as index at the name. For instance, we will write x_N or X_N to indicate the signal or its DFT, both with length N . The periodogram function estimate of the PSD (Power Spectral Density) of a signal $x_N[n]$ is:

$$\hat{P}_{xx}(f_k) = \frac{|X_N(f_k)|^2}{f_s N}, \quad (2)$$

where the frequencies are: $f_k = k \cdot f_s / N$, $k = 0, 1, 2, \dots, N-1$ in case of a complex-valued signal; $k = 0, 1, 2, \dots, N/2-1$ in case of a real-valued signal ($N = \text{even}$); $k = 0, 1, 2, \dots, (N-1)/2$ in case of real-valued signal ($N = \text{odd}$); f_s is the sampling frequency. The frequency range is: $[0, f_s/2]$ in case of a real-valued signal ($N = \text{even}$), $[0, f_s/2]$ in case of a real-valued signal ($N = \text{odd}$) and $[0, f_s]$ in case of a complex-valued signal.

It is obvious that considering a Fourier transform of a signal, it is impossible to indicate when particular events (such as drifts, trends, abrupt changes, etc.) appear within

Using spectral analysis to detect singular events

B. Duka et al.

Title Page

Abstract

Introduction

Conclusions

References

Tables

Figures



Back

Close

Full Screen / Esc

Printer-friendly Version

Interactive Discussion



Using spectral analysis to detect singular events

B. Duka et al.

Title Page

Abstract

Introduction

Conclusions

References

Tables

Figures



Back

Close

Full Screen / Esc

Printer-friendly Version

Interactive Discussion



the time-series. This deficiency can be corrected by applying the Fourier transform only to small sections of the signal at successive times, a technique called windowing the signal (Gabor, 1946) or the Short-Time Fourier Transform (STFT) (Brockwell and Davis, 2009). The STFT maps a signal into a two-dimensional function of time and frequency and can provide some information about both time and frequencies thus characterizing a particular event present in the analyzed time-series.

In order to detect particular events in long time-series of the geomagnetic field components, the secular variations (SV) or secular acceleration (SA) obtained from geomagnetic observatories, we will use the “*specgram*” function of Matlab7 software (Matlab release notes, 2004), which computes the windowed discrete-time Fourier transform of a signal using a sliding window. The spectrogram is the magnitude of this function expressed in decibel (dB). Different kinds of windows have been applied, with a different length and different overlaps, providing a sampling frequency: $f_s = 1$ (month⁻¹ or yr⁻¹ according to the kind of analysis). To avoid a plain spectrum in the case of geomagnetic field components, an average value of series is subtracted from each data input.

The most used windows have a Gaussian-like form (e.g. Blackman, Bohman, Chebyshev, Gaussian, Hamming, Hann, Parzen windows, to say some), and we notice that the results of spectrogram analyses almost do not depend on the form of window, although slightly depend on the window length and overlaps, and considerably depend on the length of the signal.

3.1.2 SFTF – applied to a signal generated by an analytical function

Mathematically, the jerk events are discontinuities (breakdowns) of the second derivatives of the geomagnetic field components. To test the real effectiveness of different techniques, we consider a synthetic signal which has such breakdowns in its second derivative. Then we will take advantage of the found results to apply the same processing scheme to real data.

Using spectral analysis to detect singular events

B. Duka et al.

Title Page

Abstract

Introduction

Conclusions

References

Tables

Figures

⏪

⏩

◀

▶

Back

Close

Full Screen / Esc

Printer-friendly Version

Interactive Discussion



We consider the following synthetic signal as defined in the interval $[-0.5, 0.5]$:

$$f(t) = \begin{cases} \exp(-4t^2) & \text{for } t \in [-0.5, 0) \\ \exp(-t^2) & \text{for } t \in [0, 0.5] \end{cases}, \quad (3)$$

and sampled at every $\Delta t = 10^{-3}$. We actually rescaled the temporal abscissa as time = $500 + t \cdot 1000$, i.e. in the interval of time 0–1000. The spectrogram of the signal does not show any breakdown, but the spectrogram of the first differences of the signal values shows the breakdown close to the real one at time = 500 (Fig. 2).

Therefore, in order to detect the geomagnetic jerks by STFT, we have to study the spectrograms of the first differences of the geomagnetic field components (SV).

3.1.3 SFTF – applied to annual series of secular variation

We present here some results of SFTF analyses, firstly applied to NGK series of 116 values long (from 1890 to 2005). In case of X-, Y-, Z-component series, from the original data an average value of the series is subtracted. Thereafter, in order to get a reliable comparison of the results, the same kind of windows and same lengths of windows and overlaps are used. The spectrograms of different components show particular events at different epochs, most of them not corresponding to the known geomagnetic jerks found in literature (e.g. Manda et al., 2010). This fact emphasizes the previous conclusion that is better to analyse the SV signals. The spectrograms of SV of X-, Y-, Z-components of NGK Observatory, calculated as the first differences of the consecutive annual means, show the evidence of particular events likely to be the geomagnetic jerks especially in the case of the Y-component (see Fig. 3).

It is obvious that spectrograms of the first differences (SV) of the field component are shifted toward the higher frequencies¹ regarding the spectrogram of the components

¹The Fourier components of a function derivative are Fourier components of the function multiplied by the frequency. The spectrograms of the second differences (SA) (not presented here) show more clear the shift toward the higher frequencies.

themselves, and one can distinguish particular events looking at the higher frequencies band. Anyway, in case of SV of Y-component there is a clear evidence of a special event around 1969, that corresponds to the first known geomagnetic jerk noted in that epoch. One can also note some evidence of geomagnetic jerks of 1901 and 1999, but not so clear evidences of other known events.

3.1.4 STFT applied to the monthly series of secular variation

In case of monthly mean value series of the geomagnetic field components, the first differences represent very irregular and noisy signals (Fig. 1). In order to minimize this noise, mainly produced by the external field variations (ionospheric and magnetospheric variations), a moving average is applied to monthly values of SV. For example, for the Y-component, less influenced by external fields, the SV is calculated as:

$$SV_y(i) = \frac{\sum_{k=0}^{n-1} Y(i+k) - \sum_{l=1}^n Y(i-l)}{n} \quad (4)$$

where $n = 1, 2, 3, 4, \dots, 12$, for different representatives of SV with different size of the running window. Usually, studies on geomagnetic jerks considered $n = 12$ -month moving average (e.g. Manda et al., 2000).

In the following we present the results for three different window sizes: $n = 6$, $n = 9$ and $n = 12$ for Y-component at NGK Observatory.

As it can be seen (Fig. 4) for all three chosen windows the global behavior is the same, but the larger running window is, the smoother and more de-noised the signal is. Thereafter, by using spectrograms, we can detect the geomagnetic jerks around the years: 1900, 1969 and 1990, the best case being when the moving window has a length of 12 months (Fig. 5).

Another way to get the monthly means by averaging the hourly means (slightly different from the classical one) is to compute SV according to Eq. (4) with $n = 6$. N. Olsen (IAGA 19th Scientific Assembly, Sopron-Hungary, 2009) has proposed the

Using spectral analysis to detect singular events

B. Duka et al.

Title Page

Abstract

Introduction

Conclusions

References

Tables

Figures



Back

Close

Full Screen / Esc

Printer-friendly Version

Interactive Discussion



is capable of revealing aspects of data like trends, breakdown points, discontinuities in higher derivatives, and self-similarity. It is also used to compress or de-noise a signal without appreciable degradation (e.g. Kumar and Georgiu, 1994).

Similar to Fourier analysis, wavelet analysis is the breaking up of a signal into shifted and scaled versions of the original (or *mother*) wavelet. The continuous wavelet transform (CWT) of a time function $s(t)$ is defined as the sum over all time of the signal multiplied by scaled and shifted versions of the wavelet function Ψ (Misiti et al., 2007):

$$c(a,b) = \int_{-\infty}^{\infty} s(t)\Psi(a,b,t)dt \quad (5)$$

with a = scale, b = position (please see also below). If a function Ψ is continuous, has null moments, decreases quickly towards 0 when t tends towards infinity, or is null outside a segment of R , it is a likely candidate to become a wavelet. Scaling a wavelet simply means stretching (or compressing) it by a scale factor a . The smaller the scale factor, the more “compressed” the wavelet. Shifting a wavelet simply means delaying (or hastening) its onset. The wavelet decomposition consists of calculating a “resemblance coefficient” between the signal and the wavelet located at position b and of scale a . The family of such coefficients $c(a,b)$ depends on two indices a and b (Kumar and Georgiu, 1994):

$$c(a,b) = \int_R s(t) \frac{1}{\sqrt{a}} \Psi\left(\frac{t-b}{a}\right) dt \quad (6)$$

In the Continuous Wavelets Transform (CWT), the set to which a and b belong is: $a \in R^+ - \{0\}$, $b \in R$. In the Discrete Wavelets Transform (DWT), the scale parameter a and the location parameter b are discrete, usually based on powers of two: $a = 2^j$, $b = k \cdot 2^j$, $(j, k) \in Z^2$ (so-called dyadic scales and positions).

Using spectral analysis to detect singular events

B. Duka et al.

Title Page

Abstract

Introduction

Conclusions

References

Tables

Figures

⏪

⏩

◀

▶

Back

Close

Full Screen / Esc

Printer-friendly Version

Interactive Discussion



We define:

$$\psi_{j,k}(t) = \frac{1}{\sqrt{2^j}} \psi\left(\frac{t - k2^j}{2^j}\right) = 2^{-j/2} \psi(2^{-j}t - k), \quad (7)$$

identifying $\Psi_{00}(t) = \Psi(t)$. It is possible to construct a certain class of wavelets $\Psi(t)$ such that $\Psi_{j,k}(t)$ are orthonormal, i.e. the wavelets are orthogonal to their dilates and translates:

$$\int \psi_{j,k}(t) \psi_{j',k'}(t) dt = \delta_{jj'} \delta_{kk'}.$$

This implies that all such functions $\Psi_{j,k}(t)$ form a complete orthonormal basis for all functions $s(t)$ that have finite norm, i.e.: the DWT $c(j,k)$ of the time signal $s(t)$ is defined such as:

$$s(t) = \sum_{j \in \mathbb{Z}} \sum_{k \in \mathbb{Z}} c(j,k) \psi_{j,k}(t), \quad \text{where } c(j,k) = \langle s, \psi_{j,k} \rangle \equiv \int s(t) \psi_{j,k}(t) dt \quad (8)$$

Let us fix j and sum on k . A detail d_j is then the function:

$$d_j(t) = \sum_{k \in \mathbb{Z}} c(j,k) \psi_{j,k}(t) \quad (9)$$

The signal is the sum of all the details:

$$s = \sum_{j \in \mathbb{Z}} d_j \quad (10)$$

Let us take now a reference level called J . There are two sorts of details. Those associated with indices $j \leq J$ correspond to the scales $a = 2^j \leq 2^J$ which are the fine details. The others, which correspond to $j > J$, are the coarser details. We group these latter details into:

$$a_J = \sum_{j > J} d_j \quad (11)$$

Using spectral analysis to detect singular events

B. Duka et al.

Title Page	
Abstract	Introduction
Conclusions	References
Tables	Figures
◀	▶
◀	▶
Back	Close
Full Screen / Esc	
Printer-friendly Version	
Interactive Discussion	



which defines what is called an approximation of the signal s . We have just created the details and an approximation. The equality:

$$s = a_J + \sum_{j \leq J} d_j \quad (12)$$

signifies that the signal s is the sum of its approximation a_J and of its fine details.

In order to better identify discontinuities in the second derivative of the geomagnetic field components (monthly mean values series) registered at different observatories, we considered different kinds of wavelet shapes and level parameters among those contained in the wavelet toolbox of Matlab software (<http://www.mathworks.com/help/toolbox/wavelet/>). We based our choices on the known criterion:

- To detect a “rupture” in the j -th derivative, select a sufficiently regular wavelet with at least j vanishing moments.

The presence of noise makes identification of discontinuities more complicated. If the first levels of the decomposition can be used to eliminate a large part of the noise, the “rupture” is sometimes visible only at deeper levels in the decomposition.

After many attempts, the wavelets, that successfully detected the second order derivative change in the known signal (3), resulted to be the Daubechies (Daubechies, 1992) wavelet of order 4 (Db4) at level 2 of the signal decomposition:

$$s = a_2 + d_2 + d_1, \quad (13)$$

where the decomposition (Eq. 12) is stopped at $J = 2$. The results show great anomalous values of the coefficients d_1 and d_2 exactly where (time = 500) the signal (3) has the second derivative breakdown. This breakdown is better localized by the anomalous values of d_1 coefficients.

Using spectral analysis to detect singular events

B. Duka et al.

Title Page

Abstract

Introduction

Conclusions

References

Tables

Figures



Back

Close

Full Screen / Esc

Printer-friendly Version

Interactive Discussion



3.2.2 Wavelets technique and its use for data de-noising

Synthetic data

In order to improve the results of the spectrogram function applied on the monthly series of SV, a signal de-noising is needed. We tried such de-noising by using the discrete wavelet analyses. To define empirically the best way to apply of such a technique, we generate a series of values with several spikes that have different changes of the slopes (Fig. 6). In order to have a signal more likely the secular variation registered in an observatory, we added to the original synthetic signal a colored noise generated by a Matlab function (warma) with some changes (extending and increasing of the warma-signal). These changes provide a more realistic noise (more like the SV signal) with the amplitude of the noise about 15 % of the signal itself. The composed signal and its spectrogram are shown in Fig. 6.

After applying DWT with different wavelets, the most appropriate ones in order to get the best de-noised signal are the Daubechies wavelets of order 3 and level 4. Such de-noised signal and its spectrogram are shown in Fig. 6. Based on the results regarding the synthetic signal (3), we can say that:

- The peaks or dips of the spikes, that are the abrupt changes of the slopes, are always identified by the maxima of the spectrograms. These maxima are as large as the spikes formed by the changes or slopes. The clear separations between maxima correspond to the middle of slopes and the dipper the slopes are, the narrower separations are.
- Defining an appropriate de-noising process and applying it to the composed signal (original one and noises), a spectrogram similar to that of the original signal is obtained. This new spectrogram can be easily used to identify the abrupt changes of slopes.

Considering that the added noise could overlap some frequencies of the original signal, and comparing the upper graphs in Fig. 6, it is clear that most of the singularities

SED

3, 615–654, 2011

Using spectral analysis to detect singular events

B. Duka et al.

Title Page

Abstract

Introduction

Conclusions

References

Tables

Figures



Back

Close

Full Screen / Esc

Printer-friendly Version

Interactive Discussion



amplitude of the detailed coefficients d_1 of the signal decomposition as a measure of the second derivative breakdown of the signal, we have calculated the averaged value of such coefficients for each year of the signal duration:

$$d_1(\text{year}(k)) = \sqrt{\frac{\sum_{i=1}^{12} (d_1(\text{year}(k), \text{month}(i)))^2}{12}} \quad (14)$$

5 Real data

Considering again the NGK observatory, a good de-noising of the monthly value series of SV without distortions of the signal itself, are achieved by using Daubechies wavelets of order 2 level 3 or level 4, of order 3 level 4, of order 4 level 5 or level 6 decompositions (see Fig. 9). From the previous tests we can conclude that the better way to detect particular events (breakdowns of the first derivative) in such de-noised series is to use the Daubechies wavelets for the wavelet decompositions of level 2 of the same order as those used for the de-noising. Plotting the averaged values of detail coefficients d_1 (Fig. 9) of such decompositions, we see that all decompositions detect the geomagnetic jerks of 1969 and 1991, while in the higher order decomposition the particular events of 1922 and 1941 appeared. This last event, not known as a local or global geomagnetic jerk, is related to changes of the SV slope due to several spikes close to each other.

We have then applied the same way of analyses for the long monthly series of 4 geomagnetic observatories mentioned in Sect. 3.2.2. The results, not presented here, show that we have to use different order and level of wavelets for the de-noising of monthly means of SV, depending on the observatory in order to get a reasonable de-noised signal. Different kinds of decompositions of the de-noised Y-component provided by the analyzed observatories underline different particular events, some of them corresponding to well-known geomagnetic jerks. However, we can note that from some observatory data, the presence of a large number of fringe (short spikes) in the de-noised signal make very difficult the detection of geomagnetic jerks. This particularity is

Using spectral analysis to detect singular events

B. Duka et al.

Title Page

Abstract

Introduction

Conclusions

References

Tables

Figures



Back

Close

Full Screen / Esc

Printer-friendly Version

Interactive Discussion



linked not only to the difference in length of geomagnetic recordings and the data quality provided by different observatories, but also to the different behavior of Y-component SV over the Globe.

3.2.4 Global analyses

5 Accepting that the amplitude variation of the detail coefficient (d_1) of the decomposition of the de-noised secular variation is an indicator of the breakdown of the second derivative of the geomagnetic field components time-series, i.e. an indicator of a geomagnetic jerk, we composed the field of averaged amplitude of such a coefficient on the Earth surface. As we need long time-series of spatially uniformly distributed SV
10 monthly values, we chose Gufm1 model to generate SV series (from 1890 to 1990) at 212 points uniformly distributed over the Earth' surface. The FORTRAN program of Gufm1 model calculates directly not only the components of the field, but even the secular variation of these components for the period of the validity of the model (from 1580 to 1990). Such a signal contains no noise as contains the SV obtained from direct
15 measurements. For a 100-yr long (1890–1990) of monthly values series of SV_γ calculated at NGK coordinates, in the better case, we achieved the wavelet decomposition of the signal by the Daubechies wavelets of order 2 at level 2, which averaged detailed d_1 coefficients are shown in the Fig. 10. In order to detect particular events, we should consider only the d_1 coefficients that have value greater than the average (0.004) value
20 of d_1 coefficients (these values are uncovered in the Fig. 10). Here, one can identify several events, that are undeniably known of global extension (1969, 1978), or may have a similar extension (1913, 1925), or seems to be local events (1906, 1919, 1949, 1958) (Alexandrescu et al., 1996; Le Huy et al., 1998). The largest event is a local one that lasts from 1942 to 1949 and has a central maximum at 1946.

25 We applied the wavelet analyses to the monthly value series of SV_γ generated by gufm1 and CM4 models at each point of the 212 points uniformly distributed over the Earth' surface. From gufm1 model we directly generate monthly values series of SV_γ for the period 1900–1990, and from CM4 model series over 1960–2002. Each

Using spectral analysis to detect singular events

B. Duka et al.

Title Page

Abstract

Introduction

Conclusions

References

Tables

Figures



Back

Close

Full Screen / Esc

Printer-friendly Version

Interactive Discussion



time-series of all 212 points is decomposed by Db2 wavelets at level 2, saving the coefficients of decomposition. Then, we calculate the squared average value of such coefficients for every year of the period 1900–1990 for Gufm1 model and for the period 1961–2002 for the CM4 model at each of 212 points over the Earth. In such a way, we have calculated and plotted the field of d_1 coefficients at different epochs over the Earth. From such plots, we can get information about the spreading and evolution of geomagnetic field jerks. As the monthly series generated by Gufm1 model are longer than the series generated by CM4 model, the analyses results appear to be better for the Gufm1 model, therefore we present here the results for this model, only.

In Fig. 11, the fields of averaged d_1 coefficient for a selection of years from the XXth century are presented at the same scale. As we plot the deviation of d_1 coefficient value from its mean value of the whole period, the white areas correspond to the regions where the d_1 values are less than the mean value and the black areas correspond to regions where the values of the d_1 coefficient is greater than the maximum of the chosen scale. The plots of whole period can be seen in the additional movie (see Supplement).

Let us discuss, with some more details, the behavior of the d_1 coefficient derived from gufm1 model. To underline its behavior over a century an animation is available. It is indeed possible to note a relatively strong field in 1901, localized in four latitude belts mainly in the low and middle latitudes, which is followed by quiet fields from 1902 to 1904. Then two small spots of a strong field appear in 1905 over the Northern Hemisphere, gradually enlarged and expanded even in the Southern Hemisphere in 1910, 1911, 1912, to be reduced again in 1913.

Two other foci of strong field start in 1917, reaching a maximum next year and being reduced to a small spot in 1920. A quiet period follows until 1925, when a strong widespread field appears, and gradually reduces over the following years, with three remaining belts getting the strongest field on 1930–1932. From 1934 to 1940 a quiet period follows, with a few small spots at different locations, however insignificant.

Using spectral analysis to detect singular events

B. Duka et al.

Title Page

Abstract

Introduction

Conclusions

References

Tables

Figures



Back

Close

Full Screen / Esc

Printer-friendly Version

Interactive Discussion



Using spectral analysis to detect singular events

B. Duka et al.

Title Page

Abstract

Introduction

Conclusions

References

Tables

Figures

◀

▶

◀

▶

Back

Close

Full Screen / Esc

Printer-friendly Version

Interactive Discussion



From 1945 a strong field wide spreads until 1949, then two large belts of longitudes characterize the period 1950–1954. Similar shifted belts appear again in 1960, after a period of almost quiet field from 1954–1959, reaching their maxima in 1964. Another period of quiet field reaching the smallest value almost everywhere in 1967, is followed

by a strong field reaching the maximum for the European area in 1969 and for a region situated in the Southern Hemisphere in 1970. Over the time period 1972–1978 a quiet field dominates with a few small spots of strong field near the south Pole. A strong field in 1978 is observed mainly in the large west and east longitude belts. A quiet field period ends in 1982 with the appearance of two local spots of strong field: one located around African continent and the other located in the large west and east latitudes. The latest one is faded gradually in the following years, while the first one reached maximum in 1985, moving thereafter toward the South Pole and splitting in two belts of strong field in 1987. The strongest field in 1990 must be considered with caution because of the cutting edge effects.

3.3 Power Spherical Harmonic Spectra (PSHS)

The spherical harmonic analysis is a representation of the geomagnetic field potential as solution of Laplace equation, so valid from Earth's surface to ionosphere. Often, it is considered also a good representation of the potential downward the core-mantle boundary (CMB), since the magnetic and electric properties of the mantle are neglected. In order to detect any relation between the known jerk events and the time changes of the spherical harmonic of different degrees, we investigate the time variations of the Mauersberger-Lowes power spectrum terms of different degrees (Lowes, 1974, 2007) extending its definition to the secular acceleration Gauss coefficients:

$$R_n^{SA} = \left(\frac{a}{r}\right)^{2n+4} (n+1) \sum_{m=0}^n \left[(\ddot{g}_n^m)^2 + (\ddot{h}_n^m)^2 \right] \quad (15)$$

with $a = 6371.2$ = mean radius of the Earth. We estimate the spatial power spectrum of the secular acceleration because, as a geomagnetic jerk is a step-like function in the

second derivative of the geomagnetic field, it can be somehow related to extremes in the power spectral density of the second derivative, R_n^{SA} .

We have used CM4 model to calculate the time-series (1960–2002) values of the secular acceleration Gauss coefficients. In the following plots, we present the time variations of R_n^{SA} for different degrees (from $n = 1$ to $n = 12$) on the Earth's surface (see Fig. 12). We do not show R_n^{SA} at the CMB because it has the same shape (the same relative minima and maxima) at both radial distances, being just the same quantity scaled by a different radial ratio $(a/r)^{2n+4}$.

In the Table 2, for each harmonics ($n = 1, \dots, 12$) we indicate by blue (or light blue) cells when the known jerk (global or local) happened at a (nearly) relative minimum of the power, by red (or orange) cells when such jerk corresponds to a (nearly) relative maximum of the power and by white cells when it does not correspond neither to a relative minimum nor maximum of the power. This extreme analysis is made because we believe that are the temporal extremes of spherical harmonic degrees that play an important role in the appearance or not of jerks.

If we look at Table 2 in terms of rows (degrees) it shows that the best coincidences of the geomagnetic jerk dates with R_n^{SA} extremes (minima or maxima) or nearly extremes (nearly minima or nearly maxima) are found for the odd degrees $n = 1, 3$ and 5 (with an exception being $n = 2$). Then, we can estimate a spreading of the geomagnetic jerks with a wavelength of: $\frac{2\pi}{n+1/2} \cdot r$ (Backus et al, 1996), i.e. from 27 000 to 7000 km on the Earth's surface. This range of spatial scales is confirmed also by the analyses of d_1 coefficient field, previously shown, where regions of the strong fields possess these spatial scales.

We do not know whether this odd degrees prevalence is just a coincidence or comes from a physical reason. We could speculate that this could come from an inherent involvement of the odd degrees in the application of the frozen-flux approximation over a hemisphere (e.g. Benton et al., 1987), but the details of why are missing at the moment and would require an extension of our work that is outside the scope the present paper.

Using spectral analysis to detect singular events

B. Duka et al.

Title Page

Abstract

Introduction

Conclusions

References

Tables

Figures

◀

▶

◀

▶

Back

Close

Full Screen / Esc

Printer-friendly Version

Interactive Discussion



References

- Alexandrescu, M., Gilbert, D., Hulot, G., Le Mouël, J.-L., and Saracco, G.: Detection of geomagnetic jerks using wavelet analysis, *J. Geophys. Res.*, 100(B7), 12557–12572, 1995.
- Alexandrescu, M., Gilbert, D., Hulot, G., Le Mouël, J. -L., and Saracco, G.: Worldwide wavelet analysis of geomagnetic jerks, *J. Geophys. Res.*, 101(B10), 21975–21994, 1996.
- Backus, G., Parker, R., and Constable, C.: *Foundation of Geomagnetism*, Cambridge University Press, 103 pp., 1996.
- Benton, E. R., Estes, R. H., and Langel, R. A.: Geomagnetic field modeling incorporating constraints from frozen flux electromagnetism, *Phys. Earth Planet. In.*, 48, 241–264, 1987.
- Bloxham, G., Zatman, S., and Dumberry, M.: The origin of geomagnetic jerks, *Nature*, 420, 65–68, 2002.
- Brockwell, P. J. and Davis, R. A.: *Time Series: Theory and Methods*, 2nd edn., Springer, 2009.
- Chambodut, A. and Manda, M.: Evidence for geomagnetic jerks in comprehensive models, *Earth Planets Space*, 57, 139–149, 2005.
- Chambodut, A., Panet, I., Manda, M., Diament, M., Holschneider, M., and James, O.: Wavelet frames: an alternative to spherical harmonic representation of potential fields, *Geophys. J. Int.*, 163(3), 875–899, 2005.
- Chau, H. D., Ducruix, J., and Le Mouël, J.-L.: Sur le caractère planétaire du saut de variation séculaire de 1969–1970, *CR. Acad. Sci. Paris*, B293, 157–160, 1981.
- Courtillot, V., Ducruix, J., and Le Mouël, J.-L.: Sur une accélération récente de la variation séculaire du champ magnétique terrestre, *CR. Acad. Sci. Paris*, D287, 1095–1098, 1978.
- Daubechies, I.: *Ten lectures on wavelets*, CBMS-NSF Regional Conference Series in Applied Mathematics, Society for Industrial and Applied Mathematics, Philadelphia, 1992.
- De Michelis, P., Cafarella, L., and Meloni, A.: Worldwide character of the 1991 geomagnetic jerk, *Geophys. Res. Lett.*, 25, 377–380, 1998.
- Gabor, D.: *Theory of communications*, *J. Inst. Elec. Eng.*, 93, 429–457, 1946.
- Jackson, A., Jonkers, A. R. T., and Walker, M. R.: Four centuries of geomagnetic secular variation from historical records, *Philos. T. R. Soc. Lond.*, 358, 957–990, 2000.
- Kumar, P. and Georgiu, E. F.: *Wavelet Analysis in Geophysics: An Introduction*, in *Wavelet Analysis and its Applications*, Academic Press, 1–43, 1994.
- Le Huy, M., Alexandrescu, M., Hulot, G., and Le Mouël, J.-L.: On the characteristics of successive geomagnetic jerks, *Earth Planets Space*, 50, 723–732, 1998.

Using spectral analysis to detect singular events

B. Duka et al.

Title Page

Abstract

Introduction

Conclusions

References

Tables

Figures



Back

Close

Full Screen / Esc

Printer-friendly Version

Interactive Discussion



Using spectral analysis to detect singular events

B. Duka et al.

Title Page

Abstract

Introduction

Conclusions

References

Tables

Figures

◀

▶

◀

▶

Back

Close

Full Screen / Esc

Printer-friendly Version

Interactive Discussion



- Lowes, F. J.: Spatial power spectrum of the main geomagnetic field, and extrapolation to the core, *Geophys. J. Roy. Astr. Soc.*, 36, 717–730, 1974.
- Lowes, F. J.: Spatial Geomagnetic Spectrum, in: *Encyclopedia of geomagnetism and paleomagnetism*, edited by: Gubbins, D. and Herrero-Bervera, E., Springer, 351–353, 2007.
- 5 MATLAB: the language of technical computing. Using MATLAB. MathWorks Inc., 2004.
- Mandea, M., Bellanger, E., and Le Mouél, J.-L.: A geomagnetic jerk for the end of the 20th century?, *Earth Planet. Sc. Lett.*, 183, 369–373, 2000.
- Mandea, M., Holme, R., Pais, A., Pinheiro, K., Jackson, A., and Verbanac, G.: Geomagnetic Jerks: Rapid Core Field Variations and Core Dynamics, *Space Sci. Rev.*, 155, 147–175, 10 2010.
- Misiti, M., Misiti, Y., Oppenheim, G., and Poggi, J. M.: *Wavelets and Their Applications*, Hermes Lavoisier, ISTE Publishing Knowledge, 2007.
- Nagao, H., Iyemori, T., Higuchi, T., and Araki, T.: Lower mantle conductivity anomalies estimated from geomagnetic jerks, *J. Geophys. Res.*, 108(B5), 2254, doi:10.1029/2002JB001786, 2003.
- 15 Olsen, N. and Mandea, M.: Investigation of a secular variation impulse using satellite data: The 2003 geomagnetic jerk, *Earth Planet. Sc. Lett.*, 255, 94–105, 2007.
- Olsen, N. and Mandea, M.: Rapidly changing flows in the Earth's core, *Nat. Geosci.*, 1, 390–394, 2008.
- 20 Olsen, N., Mandea, M., Sabaka, T. J., and Tøffner-Clausen, L.: CHAOS-2: A Geomagnetic Field Model Derived from one Decade of Continuous Satellite Data, *Geophys. J. Int.*, 179, 1477–1487, 2009.
- Oppenheim, A. V. and Schafer, R. W.: *Discrete-Time Signal Processing*, Prentice Hall, Englewood Cliffs, NJ, 1989.
- 25 Sabaka, T. J., Olsen, N., and Langel, R. A.: A comprehensive model of the quiet-time, near-Earth magnetic field: Phase 3, *Geophys. J. Int.*, 151, 32–68, 2002.
- Sabaka, T. J., Olsen, N., and Purucker, M. E.: Extending comprehensive models of the Earth's magnetic field with Ørsted and CHAMP data, *Geophys. J. Int.*, 159, 521–547, 2004.
- 30 Stewart, D. N. and Whaler, K. A.: Geomagnetic disturbance fields: an analysis of observatory monthly means, *Geophys. J. Int.*, 108, 215–223, 1992.

Using spectral analysis to detect singular events

B. Duka et al.

Table 1. The geomagnetic observatories that have been chosen as representatives for analyses.

IAGA code	Latitude	Longitude	Altitude (m)
API	$-13^{\circ}48'$	$188^{\circ}13.2'$	4
HER	$-34^{\circ}25.2'$	$19^{\circ}13.8'$	26
KAK	$36^{\circ}13.8'$	$140^{\circ}11.4'$	36
NGK	$52^{\circ}4.2'$	$12^{\circ}40.8'$	78

Title Page

Abstract

Introduction

Conclusions

References

Tables

Figures



Back

Close

Full Screen / Esc

Printer-friendly Version

Interactive Discussion



Using spectral analysis to detect singular events

B. Duka et al.

Table 2. Jerk years correspondences with extremes of R_n^{SA} terms.

	Years of presumed jerks				
	1969	1978	(1986)	1991	1999
$n = 1$	Blue	Blue	Red	Orange	Orange
$n = 2$	Yellow	Blue	White	Red	Red
$n = 3$	Blue	Blue	Orange	Orange	Red
$n = 4$	White	White	White	White	Orange
$n = 5$	Blue	Orange	Blue	Blue	Red
$n = 6$	Blue	White	Blue	White	White
$n = 7$	Red	Yellow	White	White	Red
$n = 8$	Red	White	White	White	Orange
$n = 9$	White	Blue	White	White	Orange
$n = 10$	White	White	White	White	Orange
$n = 11$	White	White	White	White	White
$n = 12$	White	White	White	White	White

Legend

- Minimum
- Nearly Minimum
- Maximum
- Nearly Maximum
- Neither maximum nor minimum

Title Page

Abstract Introduction

Conclusions References

Tables Figures

◀ ▶

◀ ▶

Back Close

Full Screen / Esc

Printer-friendly Version

Interactive Discussion



Using spectral analysis to detect singular events

B. Duka et al.

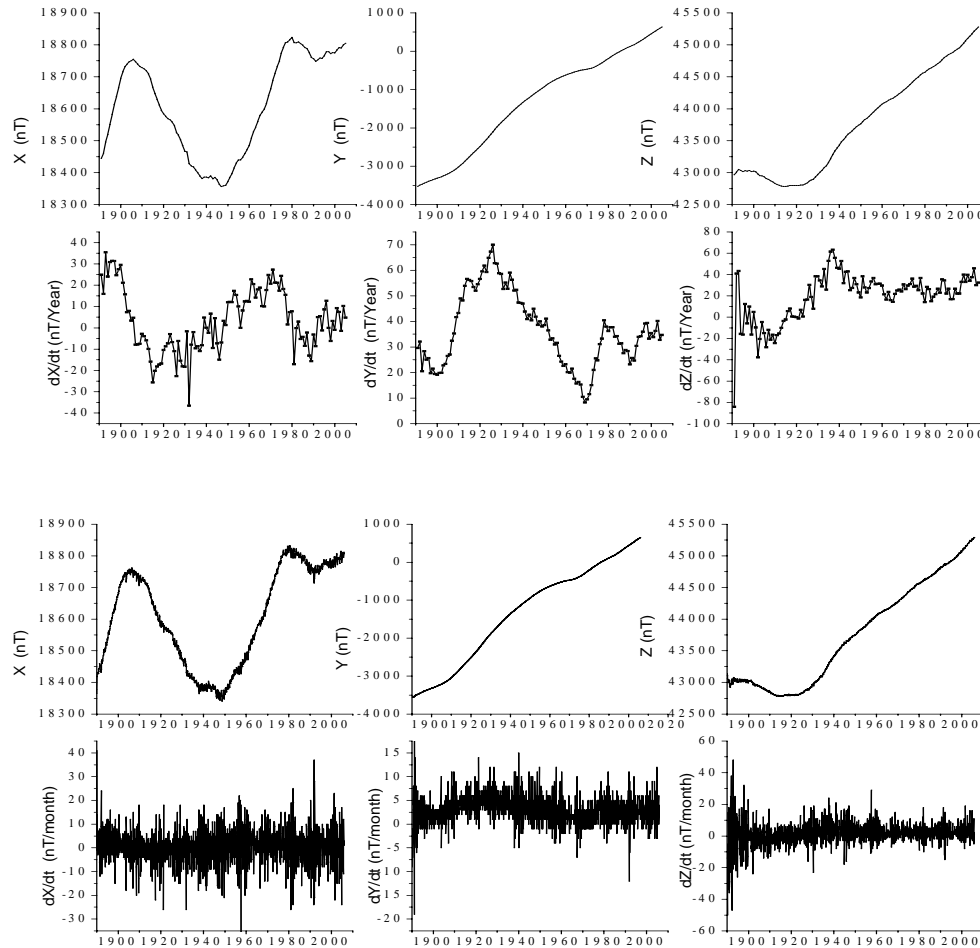


Fig. 1. Annual (up) and monthly (down) mean series of X-, Y-, Z-components and their numerical derivatives (differences of the sequential values).

Title Page

Abstract

Introduction

Conclusions

References

Tables

Figures



Back

Close

Full Screen / Esc

Printer-friendly Version

Interactive Discussion



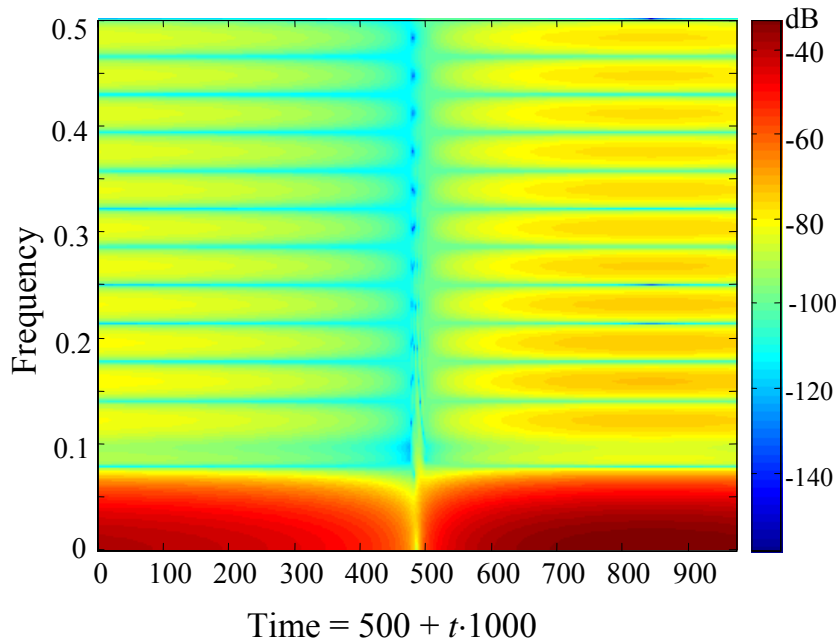


Fig. 2. The spectrogram of the first difference series of the signal (3) sampled at every $\Delta t = 10^{-3}$ with the temporal abscissa rescaled as $\text{time} = 500 + t \cdot 1000$.

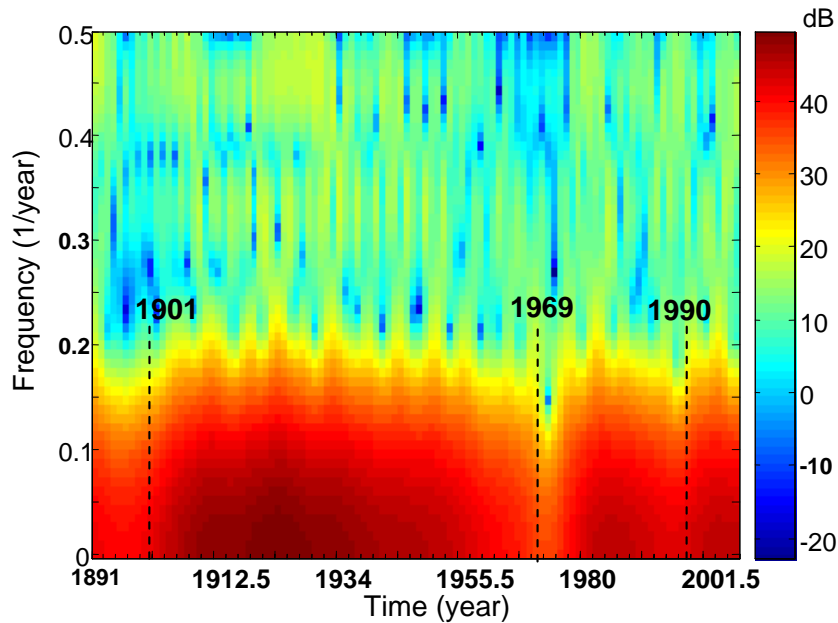


Fig. 3. Spectrogram of SV of annual mean values of Y-component recorded at NGK Observatory (1891–2005).

Using spectral analysis to detect singular events

B. Duka et al.

Title Page

Abstract

Introduction

Conclusions

References

Tables

Figures

◀

▶

◀

▶

Back

Close

Full Screen / Esc

Printer-friendly Version

Interactive Discussion



Using spectral analysis to detect singular events

B. Duka et al.

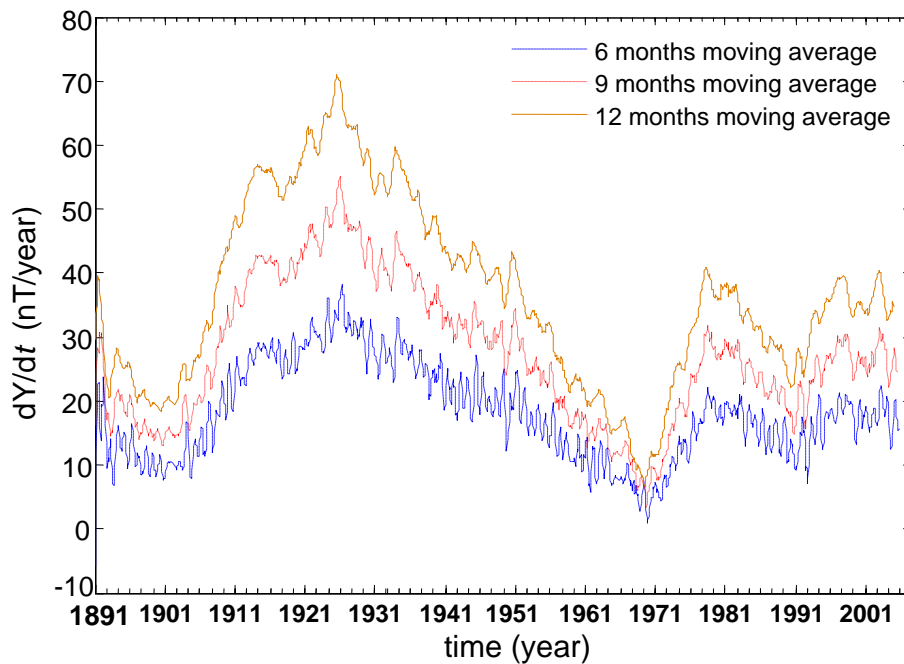


Fig. 4. Monthly values series of SV of Y-component (calculated by different moving averages) at NGK Observatory (1891–2005).

Title Page

Abstract

Introduction

Conclusions

References

Tables

Figures

◀

▶

◀

▶

Back

Close

Full Screen / Esc

Printer-friendly Version

Interactive Discussion



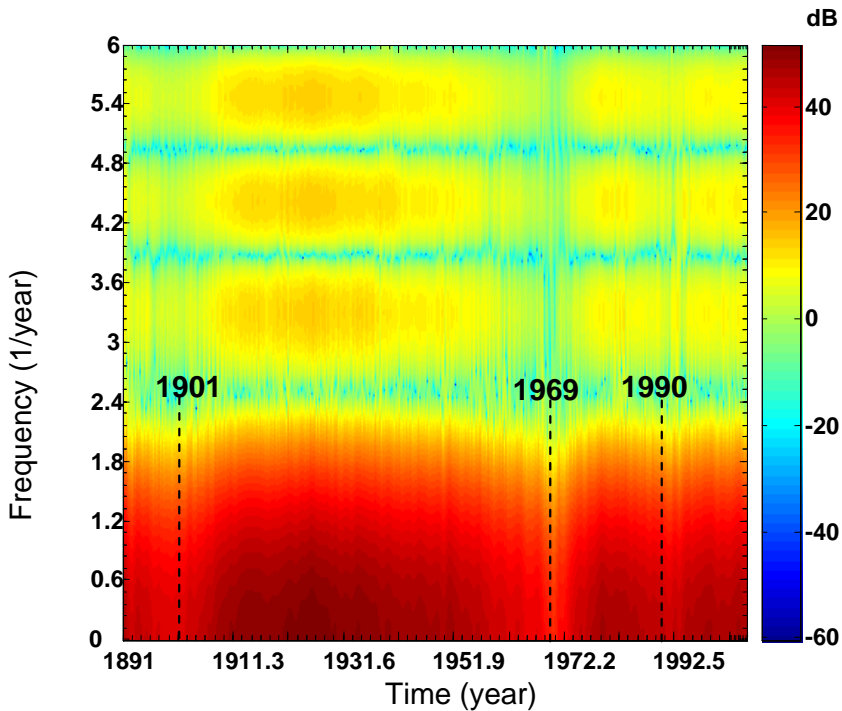


Fig. 5. Spectrogram of monthly values series of SV of Y-component (12 months moving average) at NGK Observatory (1891–2005).

Using spectral analysis to detect singular events

B. Duka et al.

Title Page

Abstract Introduction

Conclusions References

Tables Figures

◀ ▶

◀ ▶

Back Close

Full Screen / Esc

Printer-friendly Version

Interactive Discussion



Using spectral analysis to detect singular events

B. Duka et al.

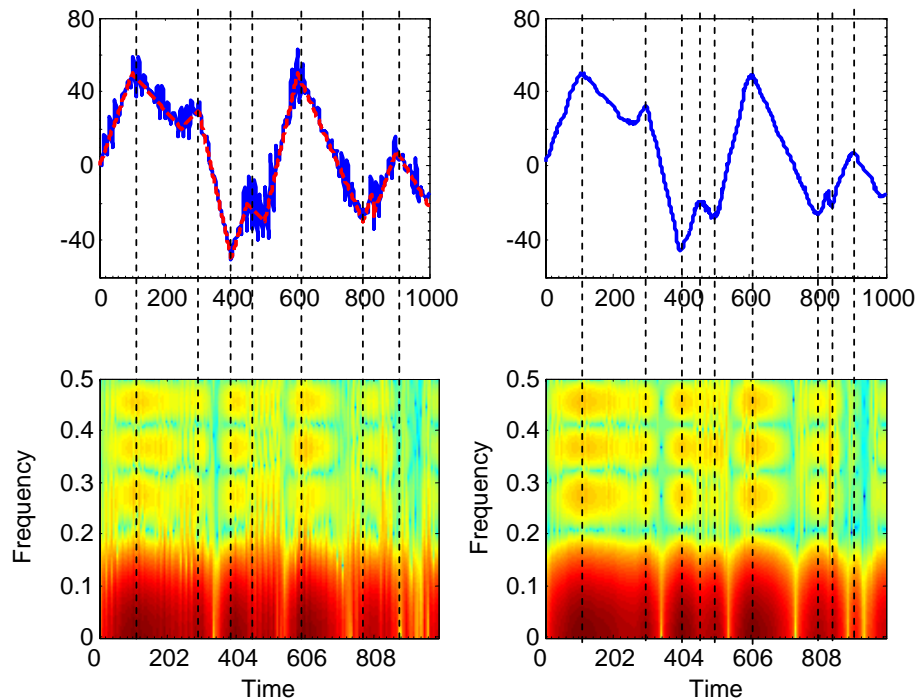


Fig. 6. Synthetic signal representing a SV-like signal (left top) composed by different spikes and a colored noise and the corresponding spectrogram (left bottom). The de-noised signal (right top) and its corresponding spectrogram (right bottom).

Full Screen / Esc

Printer-friendly Version

Interactive Discussion



Using spectral analysis to detect singular events

B. Duka et al.

Title Page

Abstract

Introduction

Conclusions

References

Tables

Figures



Back

Close

Full Screen / Esc

Printer-friendly Version

Interactive Discussion

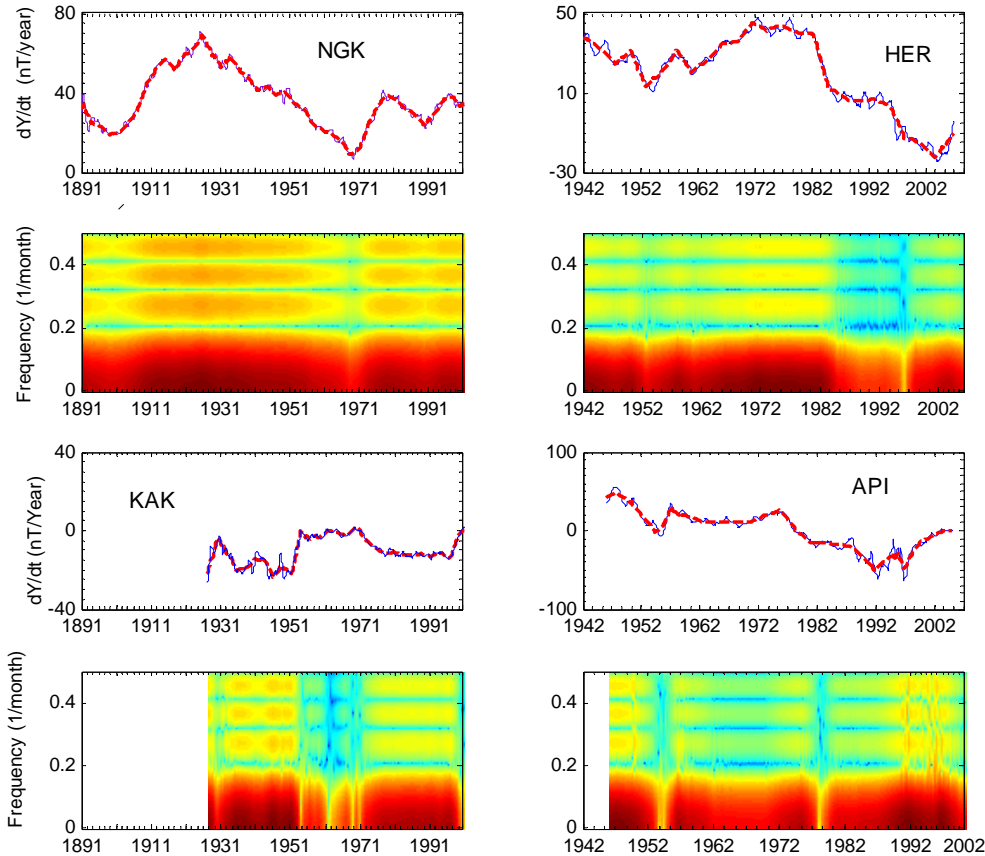


Fig. 7. The de-noised signals of secular variations ($SV_y = dY/dt$) of NGK, KAK, API and HER observatories and their respective spectrograms.

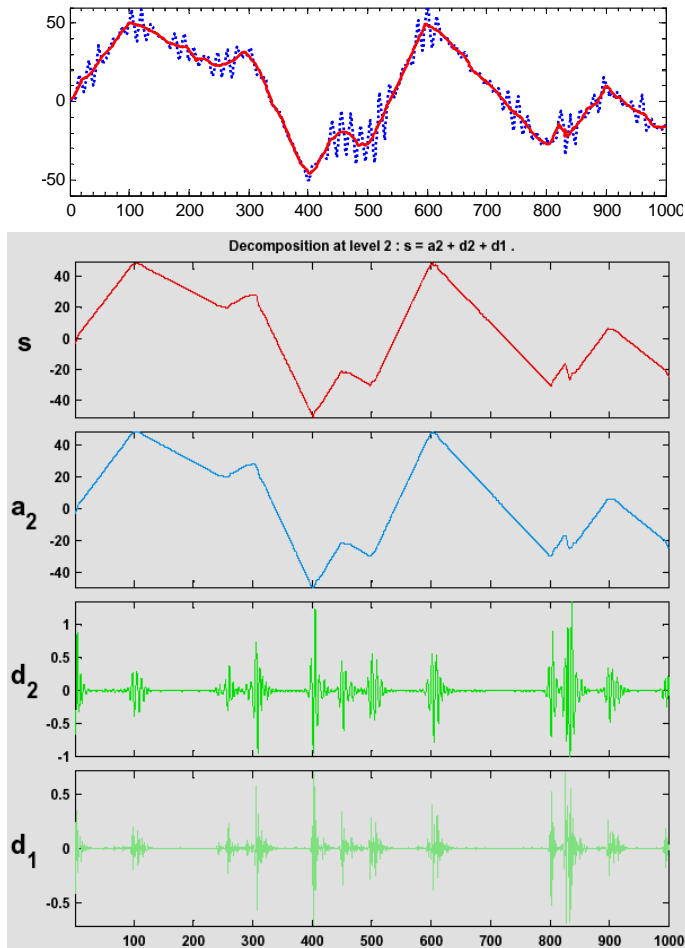


Fig. 8. The synthetic composed signal (spikes + colored noise) and its de-noised signal (up); the decomposition of the de-noised signal up to level 2 (down).

Using spectral analysis to detect singular events

B. Duka et al.

Title Page

Abstract Introduction

Conclusions References

Tables Figures

◀ ▶

◀ ▶

Back Close

Full Screen / Esc

Printer-friendly Version

Interactive Discussion



Using spectral analysis to detect singular events

B. Duka et al.

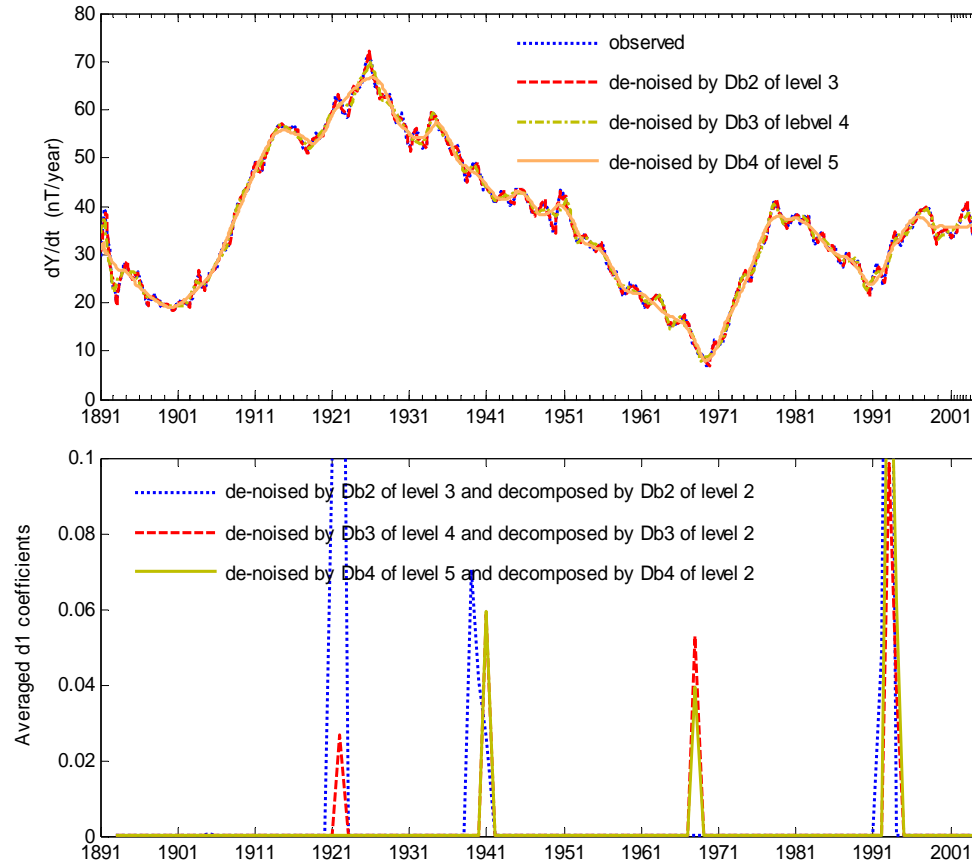


Fig. 9. De-noised SV_γ signal of NGK (up) and the respective values of averaged d_1 coefficients (down).

Title Page

Abstract

Introduction

Conclusions

References

Tables

Figures

⏪

⏩

◀

▶

Back

Close

Full Screen / Esc

Printer-friendly Version

Interactive Discussion



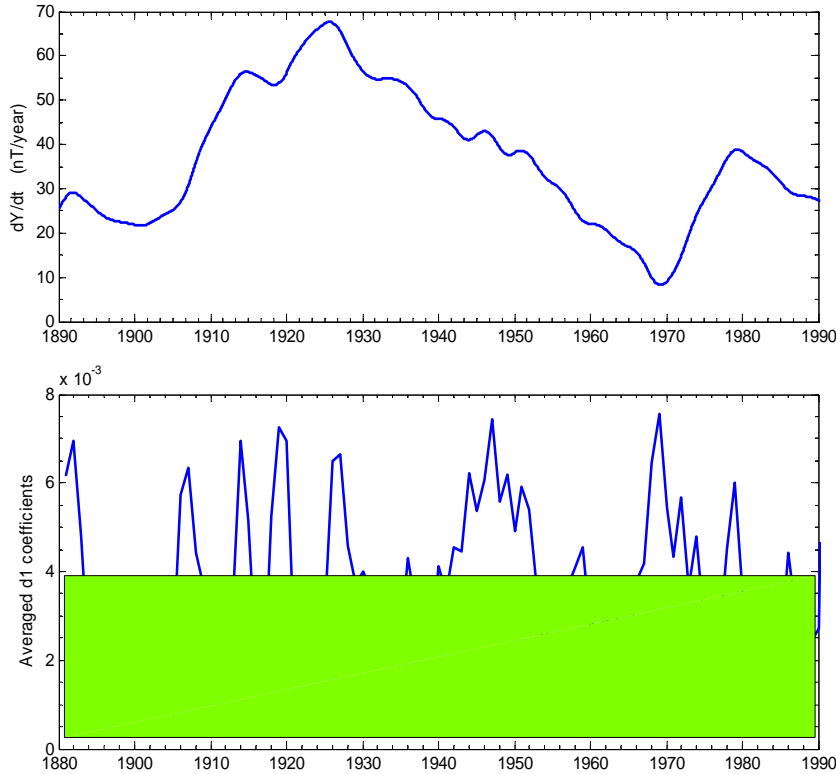


Fig. 10. Monthly value series of SV of Y-component generated by gufm1 model at NGK Observatory for the period 1890–1990 (up) and averaged d_1 coefficients of the series decomposition by Db2 wavelets of level 2. The d_1 coefficients below their mean value are hidden.

Using spectral analysis to detect singular events

B. Duka et al.

Title Page

Abstract Introduction

Conclusions References

Tables Figures

◀ ▶

◀ ▶

Back Close

Full Screen / Esc

Printer-friendly Version

Interactive Discussion



Using spectral analysis to detect singular events

B. Duka et al.

Title Page

Abstract

Introduction

Conclusions

References

Tables

Figures



Back

Close

Full Screen / Esc

Printer-friendly Version

Interactive Discussion

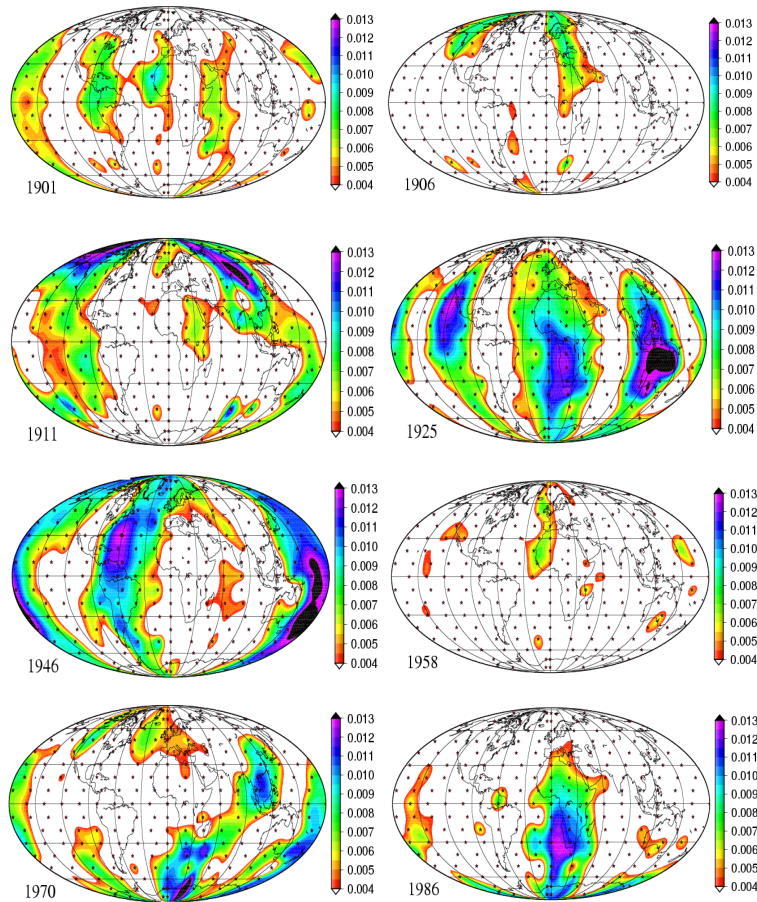


Fig. 11. An example of the d_1 coefficient field behavior, for the epochs: 1901, 1906, 1911, 1925, 1946, 1958, 1970, 1986, which are a selection from the complete movie in the Supplement.

Using spectral analysis to detect singular events

B. Duka et al.

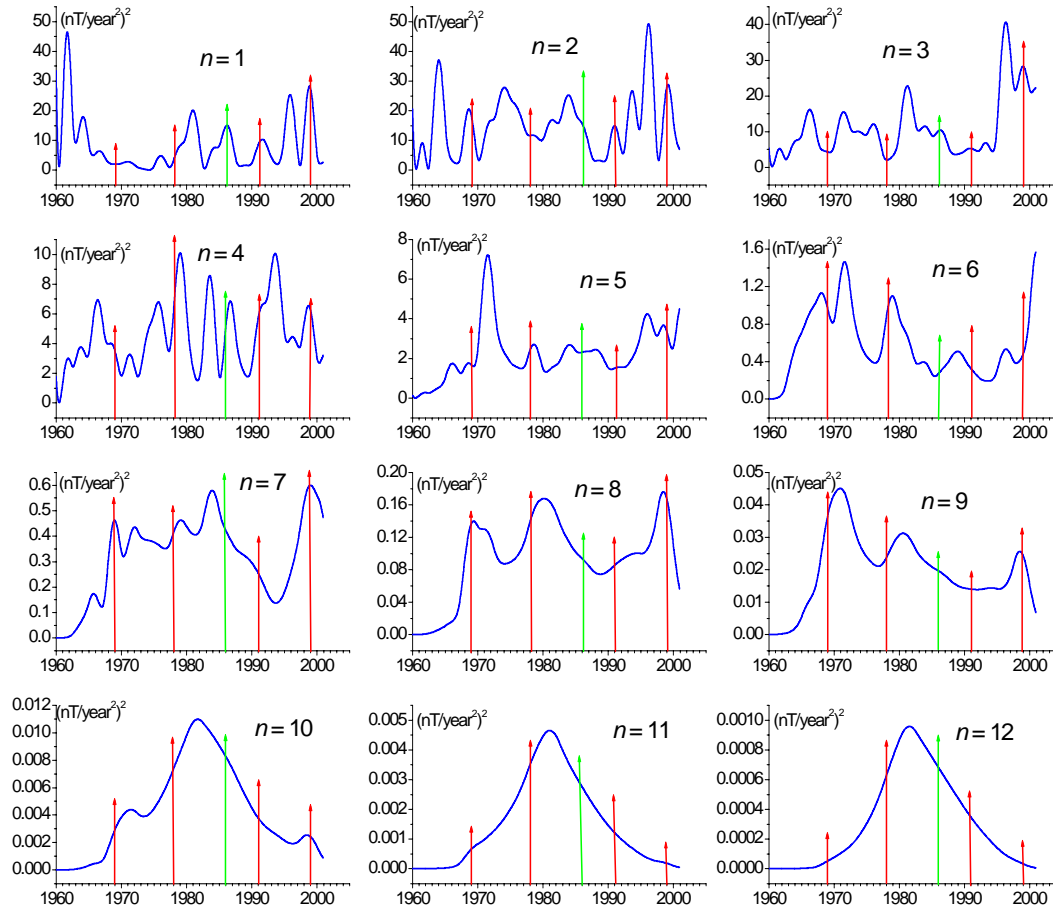


Fig. 12. Time variations of the spherical power spectra terms (R_n^{SA}) at the Earth surface.

Title Page

Abstract

Introduction

Conclusions

References

Tables

Figures

◀

▶

◀

▶

Back

Close

Full Screen / Esc

Printer-friendly Version

Interactive Discussion

